JACS
JOURNAL OF THE AMERICAN CHEMICAL SOCIETY
Article
pubs.acs.org/JACS

In Situ Assembly of Octahedral Fe(II) Complexes for the Enantiomeric Excess Determination of Chiral Amines Using Circular Dichroism Spectroscopy

Justin M. Dragna,[†] Gennaro Pescitelli,[‡] Lee Tran,[†] Vincent M. Lynch,[†] Eric V. Anslyn,*[,†] and Lorenzo Di Bari*[,‡]

[†]Department of Chemistry and Biochemistry, The University of Texas, Austin, Texas 78712, United States
[‡]Dipartimento di Chimica e Chimica Industriale, Università di Pisa, Via Risorgimento 35, 1-56126 Pisa, Italy

Supporting Information

ABSTRACT: A method for discriminating between α-chiral primary amine enantiomers is reported. The method utilizes circular dichroism (CD) spectroscopy and a sensing ensemble composed of 2-formyl-3-hydroxypyridine (**4**) and Fe(II)$(TfO)_2$. Aldehyde **4** reacts rapidly with chiral amines to form chiral imines, which complex Fe(II) to form a series of diastereomeric octahedral complexes that are CD-active in both the UV and visible regions of the spectrum. NMR studies showed that for enantiomerically pure imine complexes, the Δ-*fac* isomer is preferred. A statistical analysis of the distribution of stereoisomers accurately modeled the calibration curves for enantiomeric excess (ee). CD signals appearing in the UV region were bisignate, and the nulls of the CD signals were coincident with maxima in the UV spectrum, consistent with exciton coupling. Time-dependent density functional theory and semiempirical calculations confirmed that the CD signals in the UV region arise from coupling of the $\pi-\pi^*$ transitions in the imine chromophores and that they can be used to describe the signs and magnitudes of the curves accurately. The CD signals in the visible region arise from metal-to-ligand charge-transfer bands, and these signals can be used to determine the ee values of chiral amines with an average absolute error of ±5%. Overall, the strategy presented herein represents a facile in situ assembly process that uses commercially available simple reagents to create large optical signals indicative of ee values.

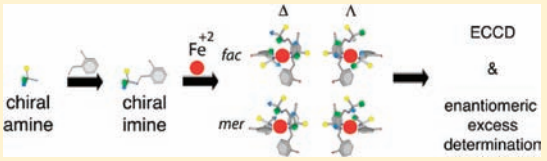

INTRODUCTION

A well-suited technique for studying chirality is circular dichroism (CD) spectroscopy.[1] Because CD spectroscopy uses a circularly polarized light source, enantiomers with absorptions in the UV−vis can be differentiated without the need for a chiral reagent.[2−4] For analytes that do not absorb in the UV−vis, it is necessary to introduce chromophores by either irreversible covalent,[5−7] reversible covalent,[8−10] or supramolecular chemistry.[11−13]

One method for introducing a chromophore into a chiral analyte is to bind the analyte to a metal, resulting in the induction or modulation of CD in the d−d transitions and/or charge-transfer bands.[14−19] Such metal-based assays are attractive because the d−d transitions and/or charge-transfer bands appear in the visible spectrum, where interference from chromophores in the analyte and/or impurities is improbable. However, such signals are often very small; additionally, it is difficult to describe metal-based systems theoretically,[14,15,17,18,20] and thus, correlations between the configuration of the analytes and the magnitude and sign of the CD signals must usually be done by empirical means.[20]

A nonempirical method first described by Nakanishi and coworkers, called exciton-coupled circular dichroism (ECCD),[1,20] has shown great utility in sensing chirality.[5−7] ECCD arises from the coupling of the excited states of at least two proximal, asymmetrically oriented chromophores. The sign of the first Cotton effect of the ECCD couplet is directly related to the sign of the dihedral angle between the transition dipoles of the chromophores, and therefore, ECCD provides insight into the configuration of the system being studied.[1]

In general, because CD spectroscopy is an optical technique, it allows for rapid analysis. Methods for rapidly distinguishing enantiomers can find applications in parallel synthesis routines for the determination of enantiomeric excess (ee).[21] Presently, determination of ee is most commonly done using chiral HPLC. Chiral HPLC is well-suited to serial asymmetric reaction discovery methods where the design and execution of reactions are the most time-intensive aspects of the discovery process. However, for parallel asymmetric reaction discovery,[22] where hundreds to thousands of reaction conditions are tested, the analysis of ee by chiral HPLC can be a bottleneck in the discovery process.

To create rapid methods for determining ee values, our group and others have implemented supramolecular and/or reversible covalent receptors in conjunction with optical instrumentation such as UV−vis, fluorescence, and CD spectroscopy.[16,23−32] Measurements taken with optical instrumentation are typically fast, allowing for high-throughput. Furthermore, the supramolecular receptors are inexpensive and can interact with

Received: December 16, 2011
Published: January 24, 2012

   dx.doi.org/10.1021/ja211768v | *J. Am. Chem. Soc.* 2012, 134, 4398−4407

a wide range of analytes. The high speeds, low cost, and wide analyte scope of supramolecular optical methods make them an attractive option for the rapid screening of ee.

Our most recently reported protocol for the determination of the ee of chiral amines uses CD spectroscopy and a sensing ensemble composed of pyridine carboxyaldehyde **1** and organometallic receptor **2** (Scheme 1).[16] Aldehyde **1** is used to convert

Scheme 1. Chiral Cu(I) Receptor and Imine Binding Scheme for Our Previously Reported Protocol:[16] A CD-Active Charge-Transfer Band Is Present in the Receptor and Modulated upon Binding of the Imine

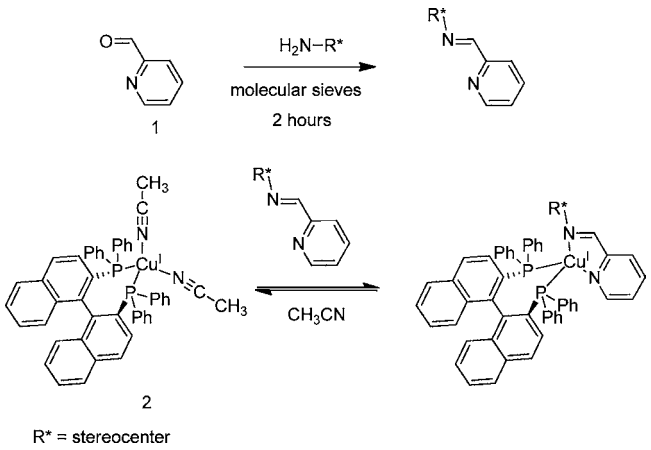

the primary chiral amines into bidentate imines. Complexation of the chiral imines with receptor **2** results in modulation of a CD-active charge-transfer band, and differential modulation of the charge-transfer band is observed for imine enantiomers with different absolute configurations. Thus, with the development of calibration curves, the system can be used to determine ee. However, the system has several limitations. First, the imine formation is slow, requiring 2 h to go to completion. Second, the CD signal appears in the UV and is of low intensity, resulting in a low signal-to-noise ratio, which leads to moderately high errors in ee of ±12%. Lastly, the calibration curves are concentration-dependent and thus require the use of an artificial neural network to relate the CD data to ee values.

Although our previous system suffers from these limitations, it is one of the few that is capable of differentiating between enantiomers of monodentate chiral primary amines. Most systems capable of differentiating amine enantiomers report results for bidentate analytes such as diamines, amino acids, and/or amino alcohols but typically do not report results for monodentate amines.[9,33−39] One recent report by Iwaniuk and Wolf[9] describes the utility of dialdehyde receptor **3** (Scheme 2). The system was designed for diamines, but fortunately, it is also applicable to the determination of chirality in monodentate amines. It was shown that for monodentate amines, the system can be used to determine ee with an absolute error of ca. 5%. The novelty of the design of **3** advances the field, but one goal of our group is to create protocols that require little to no synthesis in creating the receptor.

In the present paper, via a combination of computational and experimental methods, we explore a CD-based method for sensing chirality in monodentate amines. The method utilizes an in situ amine derivatization and self-assembly process involving commercially available materials; thus, there is no need to synthesize a receptor. This decreases the preparation time

Scheme 2. Dialdehyde Receptor Developed by Iwaniuk and Wolf[9]

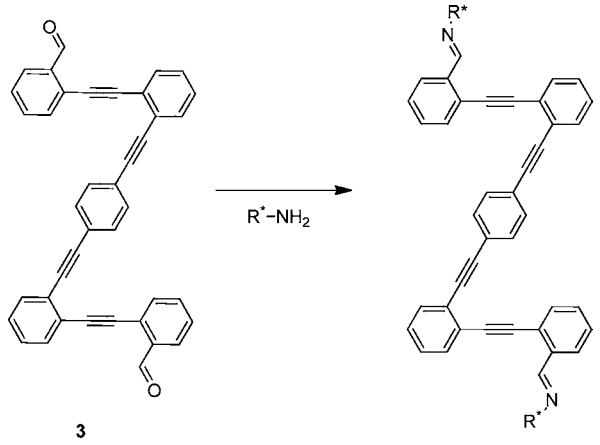

for the assay and thus increases the assay's utility to the chemistry community at large. Additionally, the protocol overcomes all of the aforementioned limitations of our previously reported method for ee determination of monodentate chiral amines.

RESULTS AND DISCUSSION

Design Criteria. To eliminate the synthesis of a host, we envisioned an assay composed of a metal ion, Fe(II), used as a scaffold and colorimetric indicator and an aldehyde, **4**, used as a chromophoric derivatizing agent for converting the monodentate amine into bidentate imine **5** in situ (Scheme 3).

Scheme 3. Aldehyde 4 Reacts Rapidly with an Amine To Form Imine 5, Followed by Complexation with Fe(II) To Form 6

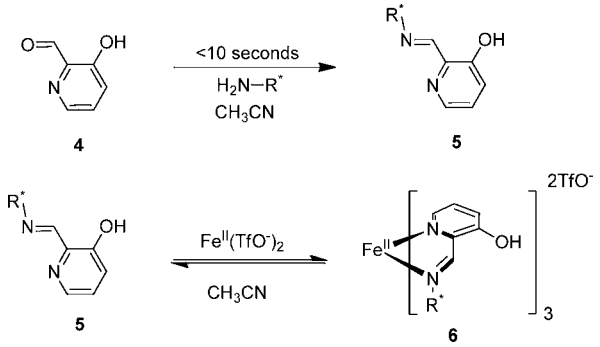

Fe(II) was chosen because it has six binding sites and thus could potentially bring 3 equiv of bidentate imine **5** into proximity to create **6**. We predicted that the proximity of the imines in **6** would allow for coupling of the $\pi-\pi^*$ transitions, giving an ECCD couplet in the UV that could be used to determine the absolute configuration. In addition, Fe(II) is known to form CD-active metal-to-ligand charge transfer (MLCT) bands in the visible range of the spectrum, which could conceivably be used in conjunction with calibration curves to calculate the ee of unknown samples.

Increasing the Rate of Imine Formation. In our previous assay, aldehyde **1** was allowed to react with a chiral primary amine to form a bidentate imine (Scheme 1). The reaction was quantitative, but it required molecular sieves and took 2 h to go to completion.[16] In the interest of speeding up this reaction, we switched to aldehyde **4** (Scheme 3). On the basis of research

dx.doi.org/10.1021/ja211768v | J. Am. Chem. Soc. 2012, 134, 4398−4407

done by Chin and co-workers[8] and Ghosn and Wolf,[10] we hypothesized that the presence of the hydroxyl group ortho to the aldehyde would increase the rate of imine formation via hydrogen bonding and/or general acid catalysis. Indeed, the addition of the hydroxyl group greatly enhanced the reactivity of the aldehyde toward amines, as the reaction of **4** to yield **5** was finished in less than 10 s. Furthermore, no molecular sieves were required to drive the reaction with **4** to completion.

Choice of Analytes and Derivatization Method. The chiral amines 2-amino-1-phenylethane (**MBA**), 1-(2-aminoethyl)-cyclohexane (**CEA**), and 2-aminoheptane (**HPA**) (Figure 1)

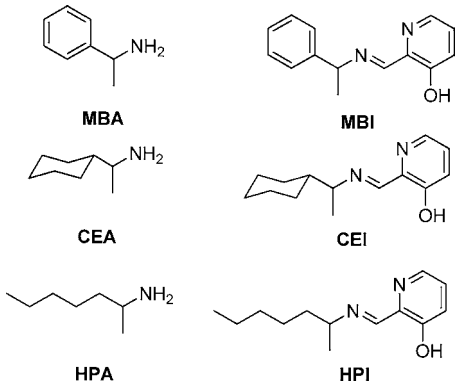

Figure 1. Structures of (left) **MBA**, **CEA**, and **HPA**, the three amines studied, and (right) **MBI**, **CEI**, and **HPI**, the three imines formed after reaction of the amines with aldehyde **4**.

were chosen for study to span a range of chemical space representing aromatic, cyclic, and aliphatic moieties, respectively. The amines were converted to the corresponding imines **5**, and then Fe(II) was added in situ, resulting in the formation of complexes **6** (Scheme 3).

Determining Saturation via UV–Vis Titrations. Titrations were performed to determine the proper ratios of **5** (**MBI**, **CEI**, and **HPI**) to Fe(II) required to reach signal saturation (Figure 2). Saturation is important because it allows for the development of concentration-independent calibration curves. As long as the assay is performed above saturation, ee calibration curves developed at a single concentration can be used to analyze unknowns at any concentration (see below). Saturation also yields the maximum signal-to-noise ratio and minimizes 2:1 and 1:1 imine:ligand species, thereby simplifying the stereochemical analysis of the CD data. The titrations revealed saturation at 3 equiv for **MBI** and **HPI**, but nearly 5 equiv was required for **CEI** because it has a lower affinity for the metal. The lower affinity of **CEI** for the metal is likely due to increased strain in the 3:1 complex as a result of the larger steric size of the cyclohexyl group of **CEI** in comparison with the steric size of the phenyl and hexyl groups of **MBI** and **HPI**, respectively. As expected, the binding curves had sigmoidal shapes, reflecting the high-order stoichiometry of the system (3:1). The imines **MBI**, **HPI**, and **CEI** show approximately the same overall change in absorption at 575, 577, and 570 nm, respectively.

Stereoisomerism. As discussed, working above saturation minimizes 2:1 and 1:1 species. Thus, the dominant complex present is the 3:1 complex of the imine with Fe(II). The complex can potentially exist as two helical isomers (Δ and Λ) and two configurational isomers (*fac* and *mer*).[40] Thus, for an enantiomerically pure sample, there are four possible stereoisomers. For amines that are not enantiomerically pure, there

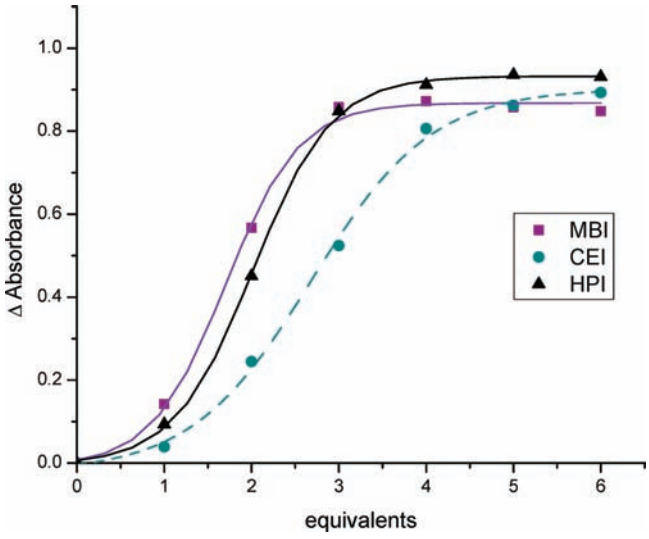

Figure 2. Changes in absorbance as functions of the number of equivalents of imine titrated into an acetonitrile solution of 1 mM Fe(II) at 575, 577, and 570 nm for **MBI**, **CEI**, and **HPI**, respectively. The number of equivalents is defined as the concentration of imine divided by the concentration of Fe(II).

are eight possible stereoisomers for the *fac* isomer and 16 possible isomers for the *mer* isomer, giving a total of 24 possible stereoisomers. Figure 3 shows the structures of all of these stereoisomers, grouped into sets based on the distribution of *R* and *S* chiral amines. The large number of stereoisomers present when mixtures of *R* and *S* amines are added to a solution of Fe(II) could result in a level of complexity that would hamper the ability to determine the ee of the chiral amines accurately. However, as long as all of the complexes are in equilibria that are rapidly exchanging and the same distribution of complexes can be reproducibly obtained, the CD spectra will be consistent and indicative of the amine ee value.

Construction of Calibration Curves. Calibration curves for ee were made by plotting the ellipticity at a single wavelength (dependent on the imine) as a function of ee at constant concentration of Fe(II) and **5** (Figure 4). To demonstrate that the calibration curves were independent of the concentration of **5** above saturation, curves were developed for **MBI** and **CEI** at multiple concentrations. As can be seen from Figure 4, there was little difference in the ellipticities at different concentrations.

The shapes of the calibration curves are sigmoidal, which we postulated could arise from some form of cooperativity between chiral imines with the same stereogenic center for binding to Fe(II). However, this postulate was ruled out. If there were such cooperativity, the shapes of the calibration curves above saturation would vary with concentration because there would be excess imines, which would thermodynamically sort to achieve the most stable isomers. As previously discussed, the shapes of the calibration curves do not vary with concentration. Thus, if there is no thermodynamic preference, the mixtures of chiral imines are most likely distributed statistically around Fe(II).

To test whether the imines were statistically distributed around Fe(II), theoretical calibration curves were developed using a probabilistic model. The first step in developing the model was to calculate the statistical distribution of isomer sets at a variety of ee values (Table 1) (see the Supporting Information for how the

dx.doi.org/10.1021/ja211768v | J. Am. Chem. Soc. 2012, 134, 4398–4407

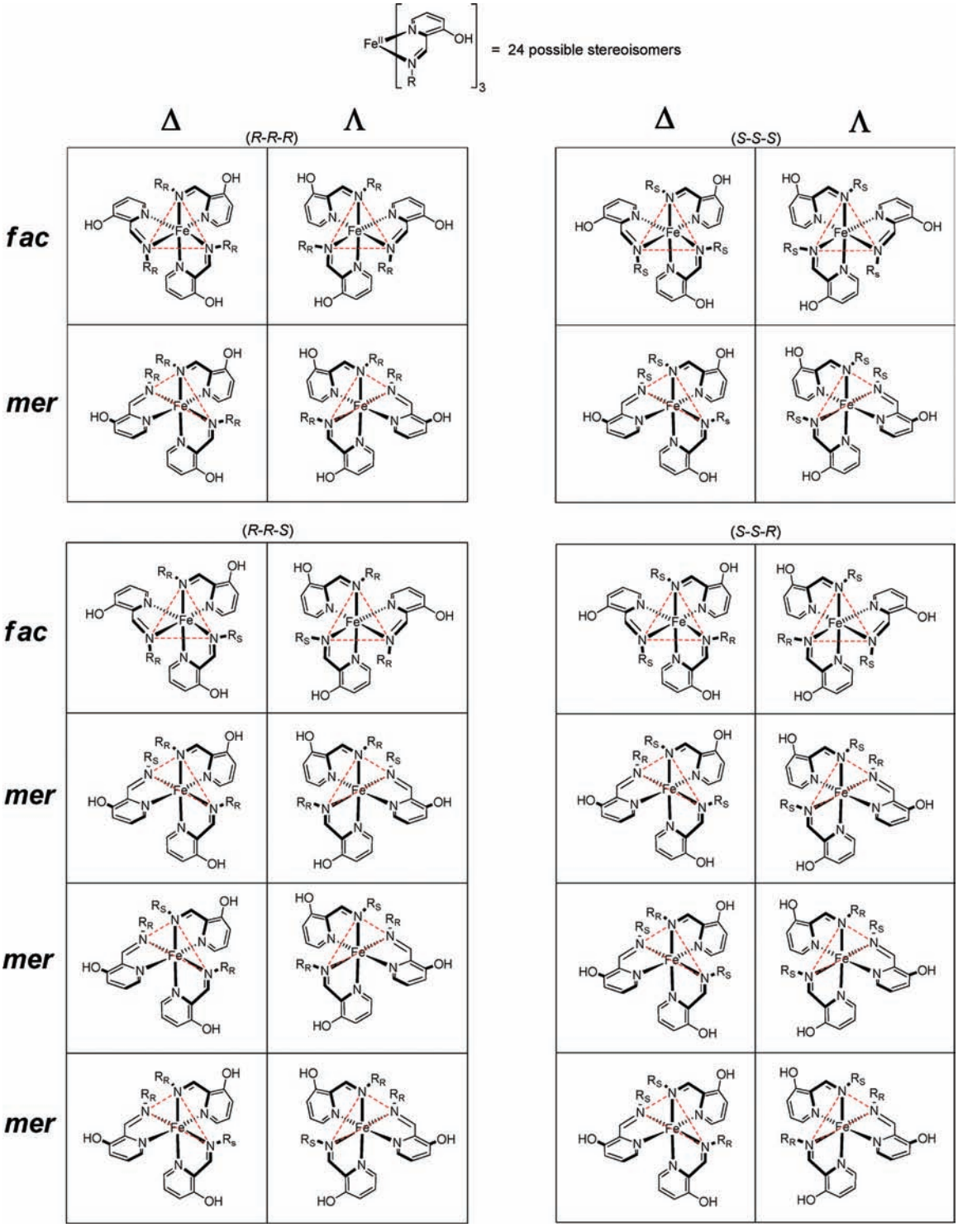

Figure 3. The 24 possible stereoisomers that can form upon mixing of enantiomers of the chiral imines with Fe(II). In this figure, the isomers are organized on the basis of the mixture of stereogenic centers on each complex [(*R*-*R*-*R*), (*S*-*S*-*S*), (*R*-*R*-*S*), and (*S*-*S*-*R*)], the configurational isomerism (*fac* and *mer*, given at the left), and the helical isomerism (Δ and Λ, given at the top). The red dotted lines trace out the "faces" and "meridians" defined by the three imine nitrogens for the *fac* and *mer* isomers, respectively.

calculations were performed). A 100% ee was defined as 1 and a −100% ee was defined as −1. Thus, for example, at 80% ee, the distribution of complexes belonging to the set (*R*-*R*-*R*) is 0.73, which means that 73% of the total concentration of complex has the configuration (*R*-*R*-*R*); in contrast, the distribution of complexes belonging to (*S*-*S*-*S*) is only 0.00074. To account for the equal and opposite nature of CD signals arising from enantiomeric pairs, a positive sign was assigned to isomers that are predominantly *R* and a negative sign was assigned to isomers that are predominantly *S*. Thus, at 80% ee, the (*R*-*R*-*R*) set has a positive value of 0.73 and the (*S*-*S*-*S*) set a negative value of −0.00074. The signs were assigned on the basis of the signs of the CD spectra of enantiomerically pure solutions of the complexes. Finally, because CD signals arising from enantiomeric

dx.doi.org/10.1021/ja211768v | *J. Am. Chem. Soc.* 2012, 134, 4398−4407

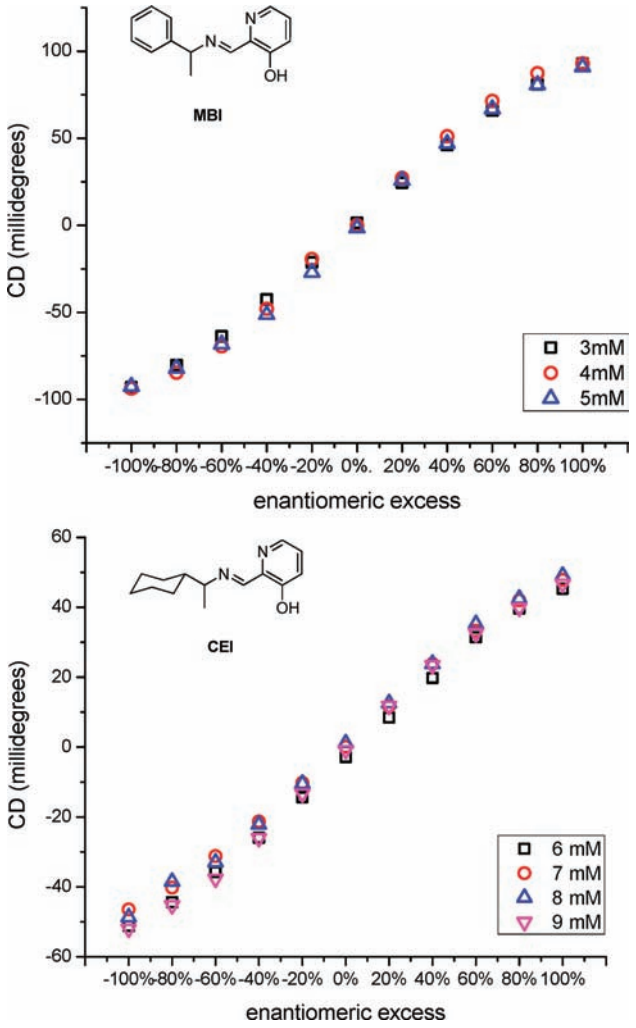

Figure 4. (top) Plots of the ellipticity at 519 nm as a function of ee with 1 mM Fe(II) and 3, 4, or 5 mM **MBI** (derived from **MBA**) in acetonitrile in a 0.1 cm cell. (bottom) Plots of the ellipticity at 525 nm as a function of ee with 1 mM Fe(II) and 6, 7, 8, or 9 mM **CEI** (derived from **CEA**) in acetonitrile in a 0.1 cm cell.

Table 1. Calculated Probabilities Spanning 100% ee to −100% ee for Different Mixtures of Chiral Imine Stereogenic Centers Surrounding Fe(II)

% ee	(*R*-*R*-*R*)	(*R*-*R*-*S*)	(*S*-*S*-*R*)	(*S*-*S*-*S*)	sum
100	1	0	0	0	1
80	0.73	0.25	−0.025	−0.00074	0.95
60	0.51	0.39	−0.094	−0.0071	0.80
40	0.34	0.45	−0.19	−0.025	0.58
20	0.21	0.44	−0.29	−0.061	0.30
0	0.12	0.38	−0.38	−0.12	0
−20	0.061	0.29	−0.44	−0.21	−0.30
−40	0.025	0.19	−0.45	−0.34	−0.58
−60	0.0071	0.094	−0.39	−0.51	−0.80
−80	0.00074	0.025	−0.25	−0.73	−0.95
−100	0	0	0	−1	−1

pairs cancel, the assigned probabilities were summed to give the overall shapes of the calibration curves.

A normalized plot of the experimental calibration curve with an overlay of the calculated calibration curve (summarized in Table 1) shows that the probabilistic model does predict the shape of the curve (Figure 5). However, the sigmoidal shape of the calculated curve is more pronounced than that of the

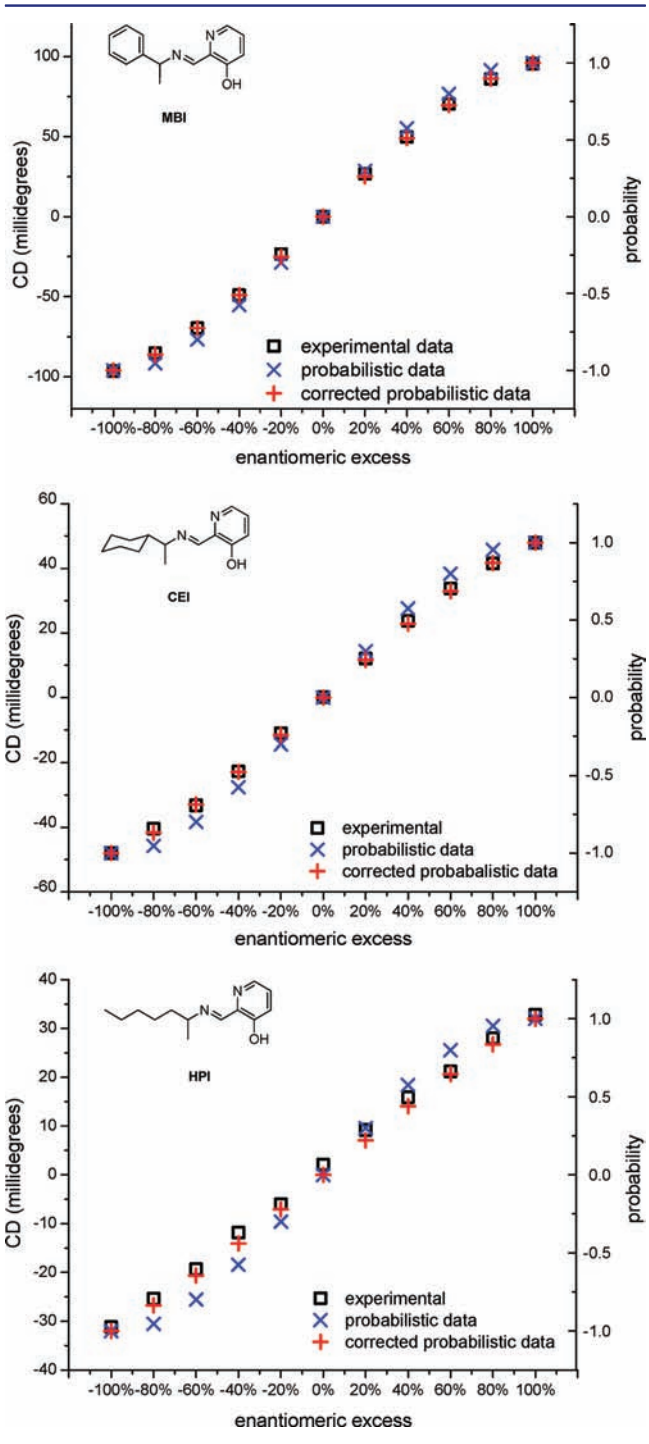

Figure 5. Overlays of the uncorrected calculated data (blue ×), corrected calculated data (red +), and experimental data (black □) for (top) **MBI**, (middle) **CEI**, and (bottom) **HPI**.

experimental curve. We postulated that the disagreement between the calculated and experimental curves arose from an assumption in the probabilistic model that the intensities of the CD signals of isomers from the sets (*R*-*R*-*R*) and (*S*-*S*-*S*) are equal to those of isomers from sets (*R*-*R*-*S*) and (*S*-*S*-*R*), respectively.

To correct for this assumption and refine the probabilistic model, the differences in the signal magnitudes were calculated

dx.doi.org/10.1021/ja211768v | *J. Am. Chem. Soc.* 2012, 134, 4398−4407

from the experimental CD data. The signal magnitudes of the sets of Fe(II) complexes for the pure isomers (*R*-*R*-*R*) and (*S*-*S*-*S*) were measured directly from the CD data using the spectra at 100% ee and −100% ee, respectively. Using the calculated probabilities, the signal magnitudes for sets (*R*-*R*-*S*) and (*S*-*S*-*R*) were calculated at each point on the calibration curve by subtracting the contributions from the pure (*R*-*R*-*R*) and (*S*-*S*-*S*) isomer sets using their distributions given in Table 1. For instance, at 80% ee, the means and standard deviations of the signals calculated for the isomer sets (*R*-*R*-*S*) and (*S*-*S*-*R*) at concentrations above saturation were 66.9 ± 6.6, 30.0 ± 2.9, and 15.8 ± 7.1 mdeg for **MBI**, **CEI**, and **HPI**, respectively. Dividing the pure-isomer ellipticity by the mixed-isomer ellipticities showed that the fractional decreases in signal in going from a pure isomer set to mixed isomer sets were 0.75, 0.62, and 0.45 for **MBI**, **CEI**, and **HPI**, respectively. These values were incorporated into the probabilistic calibration curve model by multiplying the probabilities for sets (*R*-*R*-*S*) and sets (*S*-*S*-*R*) by the respective fractional decreases. Plotting this corrected calculated signal greatly improved the agreement with the experimentally determined calibration curves, as can be seen in Figure 5. In fact, the corrected calculated curves and experimental curves virtually overlay one another.

The agreement between the probabilistic calculations and the experimental data provides strong evidence that the calibration curves indeed arise from a statistical distribution of amine stereogenic centers around Fe(II). On the basis of these results, it is expected that the induction of CD in a sensor with multiple binding sites generally will yield nonlinear calibration curves for ee.

Crystal Structure. A crystal structure of the (*S*)-**MBI**-Δ-*fac* Fe(II) complex was obtained by slow diffusion of diethyl ether into an acetonitrile solution of the interconverting complexes created with (*S*)-**MBI**. As can be seen in Figure 6, there is *π*−*π* slip-stacking between the benzyl group attached to the stereogenic center of the imine and the phenolic moiety of the parent aldehyde derivatizing agent. The crystal structure reported here is similar to that obtained for an analogous complex by Howson et al.[40]

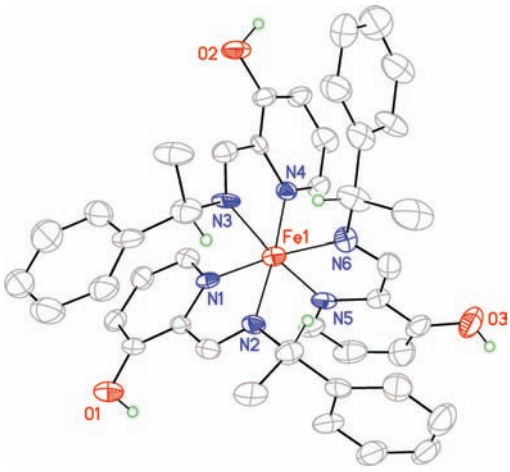

Figure 6. Crystal structure of the (*S*)-**MBI**-Δ-*fac* Fe(II) complex showing a partial atom labeling scheme. Displacement ellipsoids are scaled to the 50% probability level. Most of the H atoms have been removed for clarity.

NMR Experiments To Determine the Diastereomeric Bias. To provide a better understanding of the *fac*/*mer* diastereomeric bias of the Fe(II) complexes, ^{1}H NMR experiments were performed on the **MBI**−Fe(II) complex. Figure 7 shows the peaks corresponding to the benzylic proton of this complex at −100% ee (only the *S* isomer of **MBI**). There are two well-resolved quartets at 5.25 ppm (with the larger integral) and 4.55 ppm, which can be assigned to the C_3-symmetric *fac* species. The two broad, poorly defined multiplets between 4.70 and 5.00 ppm can be assigned to the lower-symmetry *mer* species.

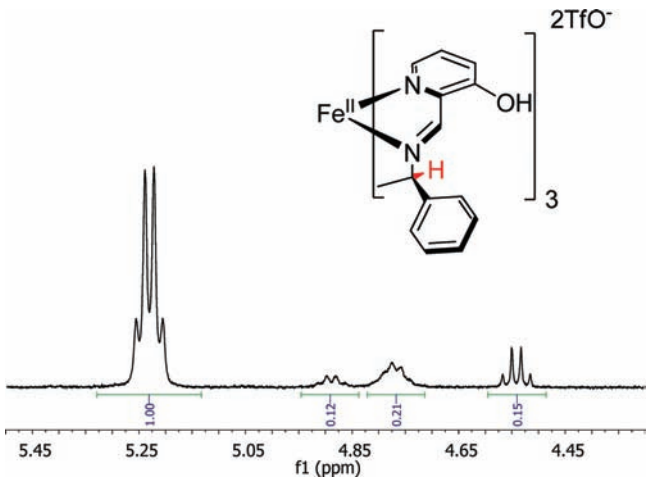

Figure 7. ^{1}H NMR spectrum (CD_3CN) of the **MBI**−Fe(II) complex at −100% ee in the region corresponding to the resonance of the benzylic proton (shown in red in the inset).

The peak in the spectrum with the largest integration (the quartet at 5.25 ppm) can be assigned to the *fac*-Δ_{Fe}-(*S*)-**MBI** isomer, which is the one isolated by crystallization and the most stable isomer found by density functional theory (DFT) (see below). The *fac*-Δ_{Fe}-(*S*)-**MBI** isomer is also in agreement with results obtained by Howson et al.[40] Consequently, the quartet at 4.55 ppm must belong to the second C_3-symmetric species, the *fac*-Λ_{Fe}-(*S*)-**MBI** isomer. On the basis of the DFT results, the two multiplets at 4.7−4.9 ppm may be assigned to the nonsymmetric *mer*-Λ_{Fe}-(*S*)-**MBI** isomer, which would have a relatively deshielded benzylic proton at 4.82 ppm and two almost-degenerate benzylic protons at ca. 4.70 ppm. In agreement with the assignment of the peak at 4.82 ppm to a single deshielded benzylic proton and the peak at 4.70 ppm to two quasi-degenerate benzylic protons, the two multiplets integrate to a 1:2 ratio, respectively. The *mer*-Δ_{Fe}-(*S*)-**MBI** isomer is either coincident with the *mer*-Λ_{Fe}-(*S*)-**MBI** isomer or is not observed because of its lower stability and thus low concentration. The DFT calculations (discussed below and shown in Figure 8) show that in comparison to the *fac*-Δ_{Fe}-(*S*)-**MBI** isomer, the benzylic protons of the *mer*-Λ_{Fe} isomer are shielded as a result of their proximity to either a pyridine (the two degenerate hydrogens) or a phenyl (Figure 8). On the basis of the assignment, we estimate a 62% diastereomeric excess for the *fac*-Δ_{Fe}-(*S*)-**MBI** isomer. ^{1}H NMR experiments were also done on enantiomerically impure imine samples (see the Supporting Information). However, the complexity of the spectra made it difficult to extract any useful information about the diastereoselectivity. The fact that at least three possible isomers are involved when an enantiomerically pure amine is used [(*S*-*S*-*S*) set in Figure 3] provides evidence that several (if not all) of the 24 possible isomers shown in Figure 3

dx.doi.org/10.1021/ja211768v | *J. Am. Chem. Soc.* 2012, 134, 4398−4407

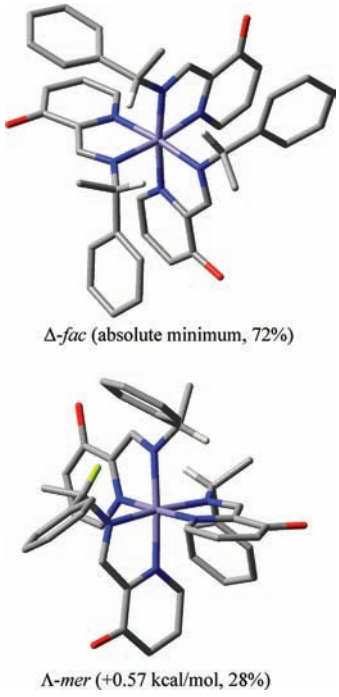

Figure 8. DFT-optimized structures of (*S*-*S*-*S*)-**MBI**−Fe(II) complexes at the BPV86/TZVP+LanL2DZ(Fe) level, with relative internal energies and Boltzmann populations at 300 K. All of the H atoms except the benzylic ones have been omitted for clarity; the H faced to phenyl is shown in yellow.

would be present within a mixture of enantiomerically impure imines.

DFT Geometry Optimizations. With the aim of rationalizing the observed NMR spectra and affording suitable input structures for the CD calculations, geometry optimizations of the **MBI**−Fe(II) complex were performed using the DFT method. First, all four possible isomers of the (*S*-*S*-*S*)-**MBI**−Fe(II) complex were generated (see Figure 3, upper right panel) starting from the X-ray geometry of the (*S*)-**MBI**-Δ-*fac* Fe(II) species (Figure 6). Next, an extensive conformational search was run with a molecular mechanics method (MMFF force field). All of the structures obtained were optimized with DFT using the BPV86 functional with a TZVP basis set for all atoms except Fe, for which the LanL2DZ basis set and effective core potential (ECP) were used (see Computational Details in the Supporting Information). The methods were based on recent literature reports on related Fe(II) complexes.[41−43] The results of the geometry optimizations are shown in Table S1 in the Supporting Information. The relevant geometries are shown in Figure 8. A highly populated single conformation was detected for each diastereomer. The calculations confirmed the *fac*-Δ_{Fe}-(*S*)-**MBI** isomer to be the most stable one, with a population of ca. 72% at 300 K. Moreover, the *mer*-Λ_{Fe}-(*S*)-**MBI** isomer was found to be the second most stable isomer (Figure 8). These findings nicely coincide with the NMR data discussed above. Conversely, the minor *fac*-Λ_{Fe}-(*S*)-**MBI** isomer was found to have a negligible population, which is at odds with NMR results. Employing different functionals (LC-BPV86, B3LYP, and M06-2X; see Computational Details) and a solvent model in the calculations did not resolve the disagreement between the computational and experimental results. The DFT-optimized structure for the *fac*-Δ_{Fe}-(*S*)-**MBI** isomer (Figure 8, top) is very similar to the X-ray geometry (Figure 6), the root-mean-square deviation between non-hydrogen atoms being 0.25 Å.

CD Spectroscopy and Exciton Analysis. The proximity and dissymmetric orientation of the three ligands surrounding Fe(II) is expected to generate ECCD signals in the region of the ligand transitions. In the UV region of the spectrum in Figure 10, bisignate CD signals are apparent with crossover points corresponding to the λ_{max} of the UV−vis spectrum around 315 nm, which is typical of exciton coupling. Quantum-mechanical calculations were performed using both time-dependent DFT (TDDFT) and semiempirical (ZINDO) methods on a model of imine **5** with R = CH_3, namely, 2-((methylimino)methyl)pyridin-3-ol (**MPI**). In all cases, a single strong electric-dipole-allowed $\pi-\pi^*$ transition at ca. 300 nm was predicted, localized on the 2-iminopyridine chromophore and directed approximately along the bond between the imine and 2-pyridine carbon atoms. The arrangement of the transition dipoles for the Δ and Λ complexes is shown in Figure 9. For octahedral D_3-symmetric tris-bidentate metal complexes with

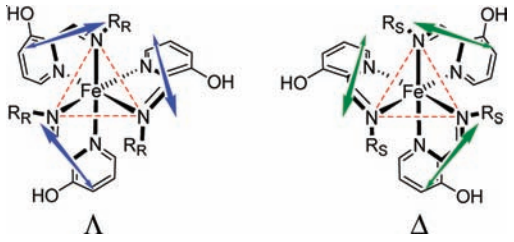

Figure 9. Helical arrangements of the transition dipoles that couple to give rise to the positive and negative ECCD couplets for the Δ-(*R*)- and Λ-(*S*)-*fac* isomers, respectively.

transition dipoles oriented parallel to the edges spanned by the ligands, exciton theory predicts the Δ configuration to be associated with a negative exciton couplet, and vice versa.[44−46] A CD couplet is defined as negative if the first or longer-wavelength Cotton effect is negative. The similarity with the present Fe(II) complexes suggests that the same correlation holds. It can be concluded that the major species observed for the **MBI**−Fe(II) complex, namely, the (*S*)-**MBI**-Δ-*fac* diastereomer, is responsible for a negative ECCD couplet around 315 nm, which is in agreement with the crystal structure and DFT geometry optimizations as well as with studies done by Howson et al.[40]

Such a conclusion may be extended to other imines too. Thus, imines with an *R* or *S* stereogenic center induce Λ or Δ helicity around Fe(II), respectively, leading to a predictable ECCD couplet (Figure 10). It can be seen in Figure 10 that the ECCD signs in the UV region correlate with the identity of the stereogenic center of the imine. Complexes containing imines with the *R* stereogenic center have a negative ECCD, couplet and those with an *S* stereogenic center have a positive ECCD couplet.

Imines derived from amines with similar functionality should follow the same pattern. As previously mentioned, the three amines span the aromatic, cyclic, and acyclic range of chemical space, and thus, it is reasonable to assume the system would behave the same with most simple α-chiral amines.

The CD signals corresponding to charge-transfer bands in the visible portion of the spectrum are also bisignate (Figure 11),

dx.doi.org/10.1021/ja211768v | *J. Am. Chem. Soc.* 2012, 134, 4398−4407

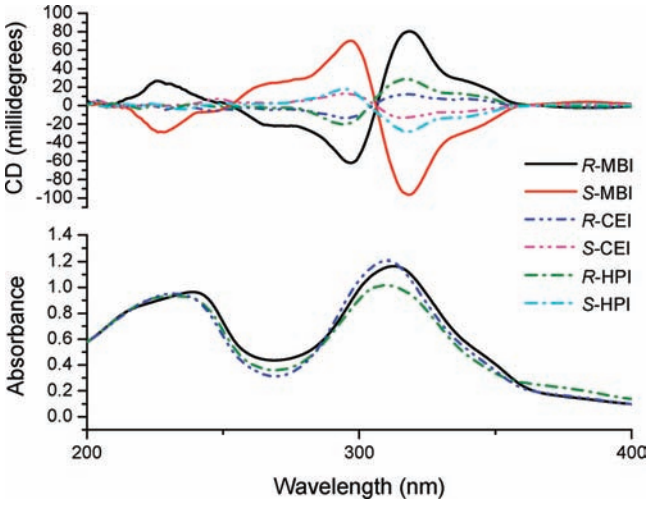

Figure 10. UV−vis and CD spectra of the MLCT bands of the three different imines studied, **MBI** (0.9 mM), **CEI** (1.8 mM), and **HPI** (2.3 mM), at 100% and −100% ee in acetonitrile with 0.3 mM Fe(II) in a 0.1 cm quartz cell from 200 to 400 nm.

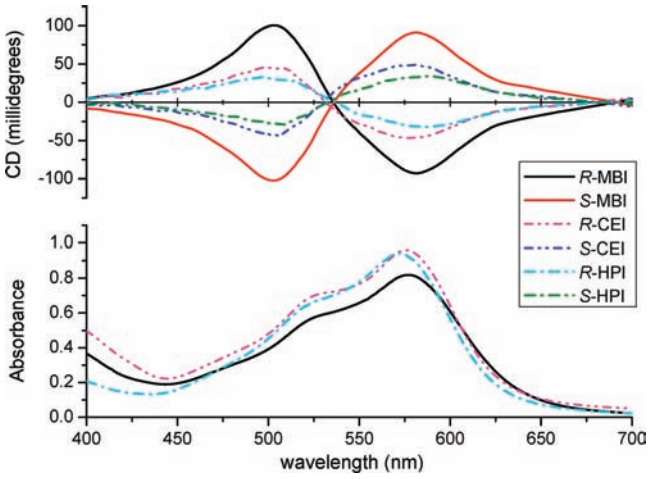

Figure 11. UV−vis and CD spectra of the MLCT bands for the three different imines studied, **MBI** (3 mM), **CEI** (6 mM), and **HPI** (7 mM), at 100% and −100% ee in acetonitrile with 1 mM Fe(II) in a 0.1 cm quartz cell from 400 to 700 nm.

and one may wonder whether they arise from an ECCD mechanism too. Interestingly enough, D_3-symmetric tris-bidentate Fe(II) complexes with typical α-diimine ligands such as 1,10-phenanthroline (phen) and 2,2′-bipyridine (bipy) also show a bisignate CD feature in the 450−600 nm region that has the same sign as the present imine complexes. In fact, Λ-$[Fe(phen)_3]^{2+}$ and Λ-$[Fe(bipy)_3]^{2+}$ both show a first negative Cotton effect around 550 nm and a second positive one around 470 nm; these are followed by a third negative Cotton effect just below 400 nm.[45] The interpretation of these CD signals is controversial, however. In particular, the CD band at the longest wavelength, which is missing in the spectra of the corresponding Ru(II) and Os(II) complexes, has been interpreted to be due to a 3d−3d transition mixed with charge-transfer ones.[45,47] The second and third CD bands are due to two d−π^* MLCT transitions, although recent TDDFT calculations have reversed the assignments of the first and third bands.[42,43] These latter reports, however, clearly demonstrate that TDDFT methods have an inherent difficulty in treating transitions involving strong participation from 3d electrons. In all cases, following these calculations, one can rule out the hypothesis that the origin of the visible CD bands of $[Fe(phen)_3]^{2+}$ and $[Fe(bipy)_3]^{2+}$ is due to exciton coupling of d−π^* transitions, as they lack the proper symmetry and/or dipole strength requirements for ECCD.[45,47]

CD Calculations. Calculations of CD spectra of Fe(II) complexes were performed using the TDDFT method[48] at the same level used for geometry optimizations, as suggested by the literature.[41−43] The input geometries for the CD calculations were obtained from the low-energy structures of the various diastereomers for (*S*-*S*-*S*)-**MBI**−Fe(II) complexes by replacing the R group with methyl [thus building the tris(**MPI**)Fe(II) complex, see Figure 12] and reoptimizing. This truncation simplified the calculations, which otherwise would have been excessively demanding, and it was justified by the similarity between all of the CD spectra for the various imine ligands (Figures 10 and 11), which demonstrates that the R groups provide weak spectroscopic contributions. The calculated CD spectrum for the Δ-*fac* diastereomer of the **MPI**−Fe(II) complex is shown in Figure 12. In the UV region, it nicely

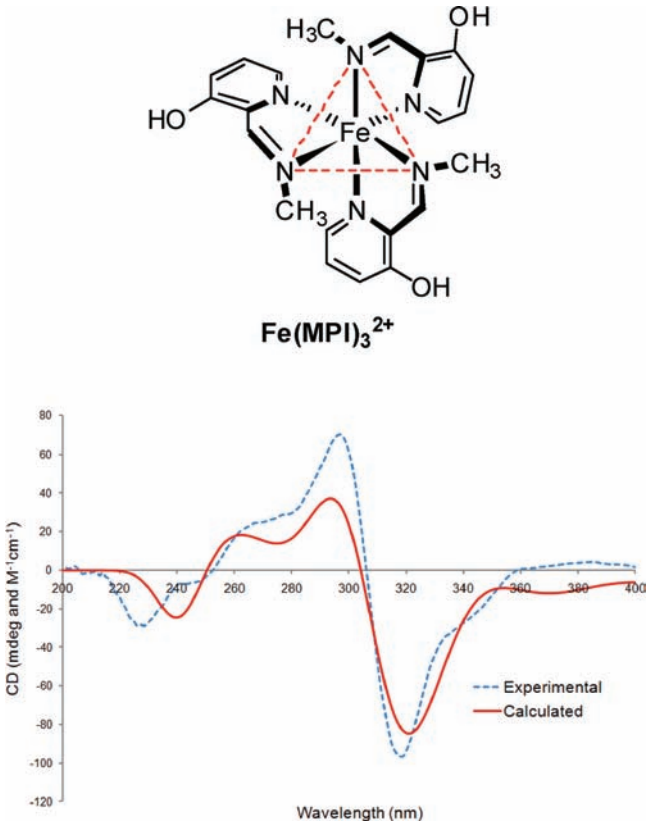

Figure 12. TDDFT-calculated CD spectrum of the Δ-*fac* **MPI**−Fe(II) complex (shown in the diagram), calculated at BPV86/TZVP +LanL2DZ(Fe)//BPV86/TZVP+LanL2DZ(Fe) level (red), compared with the experimental CD spectrum for the (*S*-*S*-*S*)-**MBI**−Fe(II) complex (blue). The calculated spectrum is a sum of Gaussians with exponential half widths of 0.22 eV and is blue-shifted by 25 nm.

reproduces the main experimental features, in particular, the negative ECCD couplet around 315 nm, further confirming the absolute configuration of the complex as established by the exciton analysis above. Importantly, when other diastereomers were considered in the calculations (not shown), the average

dx.doi.org/10.1021/ja211768v | J. Am. Chem. Soc. 2012, 134, 4398−4407

Table 2. Actual ee's Calculated from Enantiomerically Pure Solutions and Experimental ee's Determined Using the Assay

analyte	concentration (mM)	actual ee	exptl ee	absolute error
MBI	3.2	−51.0	−48.9	2.1
	3.2	32.0	30.3	1.7
	3.5	−58.0	−52.6	5.4
	3.5	38.0	35.0	3.0
	4.1	−56.0	−48.7	7.3
	4.1	75.6	68.7	6.9
	4.3	−51.0	−46.2	4.8
	4.3	22.0	20.2	1.8
	5	−30.0	−25.4	4.6
	5	52.0	47.3	4.7
analyte	concentration (mM)	actual ee	exptl ee	absolute error
CEI	7.2	−75.0	−62.0	13.0
	7.2	45.0	38.5	6.5
	7.5	−66.2	−58.7	7.5
	7.5	−68.6	−61.2	7.4
	8.3	−28.2	−28.5	0.3
	8.3	84.8	79.6	5.2
	8.6	10.4	9.0	1.4
	8.6	100	100.4	0.4
	9	30.0	30.4	0.4
	9	−52.0	−60.3	8.3
analyte	concentration (mM)	actual ee	exptl ee	absolute error
HPI	4.2	−57.2	−63.5	6.3
	4.2	71.4	60.9	10.5
	4.6	−11.6	−14.9	3.3
	4.6	35.0	28.8	6.2
	5.3	−77.2	−78.0	0.8
	5.3	47.8	42.3	5.5
	5.6	−57.0	−62.3	5.3
	5.6	29.0	21.8	7.2
	6.0	−10.0	−18.5	8.5
	6.0	−80.0	−85.6	5.6

calculated spectrum still showed a negative couplet in the ligand UV region. Population analysis and inspection of the relevant Kohn−Sham orbitals support the ECCD nature of the spectrum in this region. In fact, all transitions computed between 280 and 330 nm are mainly combinations of ligand-centered $\pi-\pi^*$ excitations. Moreover, the two transitions with the largest opposite rotational strengths (negative at 300 nm and positive at 325 nm) have different symmetries (E and A, respectively, of the C_3 point group), as required for ECCD.

In the visible region, the calculations also led to a bisignate CD feature, though it had the opposite sign with respect to the experimental spectrum as far as the Δ-*fac* diastereomer is concerned (not shown). The discrepancy was not alleviated after considering the contributions from other diastereomers. Similar failures in CD TDDFT predictions in the MLCT region have been observed for $[Fe(phen)_3]^{2+}$ and $[Fe(bipy)_3]^{2+}$ in comparison with Ru(II) and Os(II) complexes[42,43] and have been extensively discussed by the authors. For our purposes, it is interesting to note that population and orbital analysis revealed that the two calculated CD bands between 500 and 700 nm both arise from the combination of d-to-π^* transitions involving the two lowest-energy and degenerate dπ orbitals. Moreover, both transitions have the same symmetry (E) and therefore cannot represent two ECCD components.

Enantiomeric Excess Determination. As discussed above, calibration curves were constructed for all three imines by varying the ee at concentrations above saturation. The curves were fit using the Microsoft Excel. Because the shapes of the curves were sigmoidal, third-degree polynomial regression was used for fitting.

Unknowns for all three imines at a variety of ee values and concentrations were prepared. The primary optical data were input into the third-degree polynomial and used to solve for ee. The results (summarized in Table 2) further demonstrate the concentration independence of the calibration curves. If the calibration curves were concentration-dependent, it would be expected that the error would be lowest for the calculation of ee at or near the concentrations from which the calibration curve was developed. However, this was not observed. For example, the calibration curve for **HPI** was developed at 6 mM, and the absolute error was lower for test samples not done at 6 mM (Table 2).

The average absolute error for the assay was calculated and determined to be ±5%. As discussed in previously published work,[30,32] we consider an absolute error even as large as ±15% to be useful in a rapid screening protocol. The accuracy of the system reported here is well within that limit.

SUMMARY

There were several shortcomings with our previously reported assay for the determination of the absolute configuration and ee of chiral amines (Scheme 1), namely, slow formation of the imine, the need for host synthesis, moderately high error, and the required use of an artificial neural network to calculate the ee at different concentrations. To overcome the slow imine formation, aldehyde **4** was used instead of **1**, which reduced the time for imine formation from several hours to 10 s. The need for host synthesis was replaced by using self-assembly to bring together several chromophores with Fe(II). The moderately high error associated with our previous system was overcome by increasing the signal-to-noise ratio by using a strongly absorbing charge-transfer band present in **6** to develop calibration curves and analyze unknowns. Lastly, an artificial neural network was not necessary because the present assay is concentration-independent above saturation, as determined by UV−vis titrations.

The calibration curves developed for the system had a sigmoidal shape, and it was shown that the shape arises from a probabilistic distribution of stereogenic centers around Fe(II). The major species for the tris(imine)Fe(II) complex were characterized by NMR and DFT geometry optimizations. A CD-active UV band could be used to determine the absolute configuration of the amines by correlation with the sign of the ECCD couplet. The correlation was proved by exciton-chirality analysis and TDDFT CD calculations. A charge-transfer band in the visible region could be used to develop calibration curves for the determination of the ee's of unknown samples with an average accuracy of ±5%. Currently, the protocol is being transitioned to aid in the discovery of asymmetric catalysts in collaboration with synthetic methodology chemists.

ASSOCIATED CONTENT

Supporting Information

Experimental details for the preparation of calibration curves, calculations of probabilities and CD curves in the visible region, NMR data, crystallographic data (CIF), and computational

dx.doi.org/10.1021/ja211768v | J. Am. Chem. Soc. 2012, 134, 4398−4407

details. This material is available free of charge via the Internet at http://pubs.acs.org.

AUTHOR INFORMATION

Corresponding Author

anslyn@austin.utexas.edu and ldb@dcci.unipi.it

Notes

The authors declare no competing financial interest.

ACKNOWLEDGMENTS

Financial support from NIH (GM77437) and the Welch Foundation (F-1151) is acknowledged. The authors thank Damien Jouvenot for informal conversations with J.D. that led to the initial idea for this project and James Canary for putting E.V.A. in contact with L.D.B. J.D. thanks Professor Bruce Gibb.

REFERENCES

(1) Nakanishi, K.; Berova, N. In *Circular Dichroism: Principles and Applications*; Nakanishi, K., Berova, N., Woody, R. W., Eds.; VCH: New York, 1994; p 361.

(2) Boeckman, R. K.; Ferreira, M. D. R.; Mitchell, L. H.; Shao, P. C. *J. Am. Chem. Soc.* **2002**, *124*, 190.

(3) Benohoud, M.; Leman, L.; Cardoso, S. H.; Retailleau, P.; Dauban, P.; Thierry, J.; Dodd, R. H. *J. Org. Chem.* **2009**, *74*, 5331.

(4) Batista, J. M.; Batista, A. N. L.; Rinaldo, D.; Vilegas, W.; Ambrosio, D. L.; Cicarelli, R. M. B.; Bolzani, V. S.; Kato, M. J.; Nafie, L. A.; Lopez, S. N.; Furlan, M. *J. Nat. Prod.* **2011**, *74*, 1154.

(5) Matile, S.; Berova, N.; Nakanishi, K.; Novkova, S.; Philipova, I.; Blagoev, B. *J. Am. Chem. Soc.* **1995**, *117*, 7021.

(6) Harada, N.; Nakanishi, K. *J. Am. Chem. Soc.* **1969**, *91*, 3989.

(7) Cai, G.; Bozhkova, N.; Odingo, J.; Berova, N.; Nakanishi, K. *J. Am. Chem. Soc.* **1993**, *115*, 7192.

(8) Kim, H.; So, S. M.; Yen, C. P.-H.; Vinhato, E.; Lough, A. J.; Hong, J.-I.; Kim, H.-J.; Chin, J. *Angew. Chem., Int. Ed.* **2008**, *47*, 8657.

(9) Iwaniuk, D. P.; Wolf, C. *J. Am. Chem. Soc.* **2011**, *133*, 2414.

(10) Ghosn, M. W.; Wolf, C. *J. Am. Chem. Soc.* **2009**, *131*, 16360.

(11) Yashima, E.; Nimura, T.; Matsushima, T.; Okamoto, Y. *J. Am. Chem. Soc.* **1996**, *118*, 9800.

(12) Yashima, E.; Matsushima, T.; Okamoto, Y. *J. Am. Chem. Soc.* **1997**, *119*, 6345.

(13) Li, X.; Borhan, B. *J. Am. Chem. Soc.* **2008**, *130*, 16126.

(14) Dillon, J.; Nakanishi, K. *J. Am. Chem. Soc.* **1975**, *97*, 5409.

(15) Dillon, J.; Nakanishi, K. *J. Am. Chem. Soc.* **1975**, *97*, 5417.

(16) Nieto, S.; Dragna, J. M.; Anslyn, E. V. *Chem.—Eur. J.* **2010**, *16*, 227.

(17) Dillon, J.; Nakanishi, K. *J. Am. Chem. Soc.* **1974**, *96*, 4059.

(18) Dillon, J.; Nakanishi, K. *J. Am. Chem. Soc.* **1974**, *96*, 4055.

(19) Di Bari, L.; Lelli, M.; Pintacuda, G.; Salvadori, P. *Chirality* **2002**, *14*, 265.

(20) Berova, N. *Chirality* **1997**, *9*, 395.

(21) Traverse, J. F.; Snapper, M. L. *Drug Discovery Today* **2002**, *7*, 1002.

(22) de Vries, J. G.; Lefort, L. *Chem.—Eur. J.* **2006**, *12*, 4722.

(23) Shabbir, S. H.; Regan, C. J.; Anslyn, E. V. *Proc. Natl. Acad. Sci. U.S.A.* **2009**, *106*, 10487.

(24) Zhu, L.; Zhong, Z. L.; Anslyn, E. V. *J. Am. Chem. Soc.* **2005**, *127*, 4260.

(25) Nieto, S.; Lynch, V. M.; Anslyn, E. V.; Kim, H.; Chin, J. *J. Am. Chem. Soc.* **2008**, *130*, 9232.

(26) Shabbir, S. H.; Joyce, L. A.; da Cruz, G. M.; Lynch, V. M.; Sorey, S.; Anslyn, E. V. *J. Am. Chem. Soc.* **2009**, *131*, 13125.

(27) Leung, D.; Anslyn, E. V. *Org. Lett.* **2011**, *13*, 2298.

(28) Nieto, S.; Lynch, V. M.; Anslyn, E. V.; Kim, H.; Chin, J. *Org. Lett.* **2008**, *10*, 5167.

(29) Joyce, L. A.; Maynor, M. S.; Dragna, J. M.; da Cruz, G. M.; Lynch, V. M.; Canary, J. W.; Anslyn, E. V. *J. Am. Chem. Soc.* **2011**, *133*, 13746.

(30) Leung, D.; Anslyn, E. V. *J. Am. Chem. Soc.* **2008**, *130*, 12328.

(31) Zhu, L.; Shabbir, S. H.; Anslyn, E. V. *Chem.—Eur. J.* **2007**, *13*, 99.

(32) Leung, D.; Folmer-Andersen, J. F.; Lynch, V. M.; Anslyn, E. V. *J. Am. Chem. Soc.* **2008**, *130*, 12318.

(33) Ghosn, M. W.; Wolf, C. *Tetrahedron* **2010**, *66*, 3989.

(34) Li, X.; Tanasova, M.; Vasileiou, C.; Borhan, B. *J. Am. Chem. Soc.* **2008**, *130*, 1885.

(35) Kim, H.; So, S. M.; Yen, C. P.-H.; Vinhato, E.; Lough, A. J.; Hong, J.-I.; Kim, H.-J.; Chin, J. *Angew. Chem., Int. Ed.* **2008**, *47*, 8657.

(36) Huang, X. F.; Fujioka, N.; Pescitelli, G.; Koehn, F. E.; Williamson, R. T.; Nakanishi, K.; Berova, N. *J. Am. Chem. Soc.* **2002**, *124*, 10320.

(37) Kurtan, T.; Nesnas, N.; Li, Y. Q.; Huang, X. F.; Nakanishi, K.; Berova, N. *J. Am. Chem. Soc.* **2001**, *123*, 5962.

(38) Kurtan, T.; Nesnas, N.; Koehn, F. E.; Li, Y. Q.; Nakanishi, K.; Berova, N. *J. Am. Chem. Soc.* **2001**, *123*, 5974.

(39) Huang, X. F.; Rickman, B. H.; Borhan, B.; Berova, N.; Nakanishi, K. *J. Am. Chem. Soc.* **1998**, *120*, 6185.

(40) Howson, S. E.; Allan, L. E. N.; Chmel, N. P.; Clarkson, G. J.; van Gorkum, R.; Scott, P. *Chem. Commun.* **2009**, 1727.

(41) Rudolph, M.; Autschbach, J. *J. Phys. Chem. A* **2011**, *115*, 2635.

(42) Le Guennic, B.; Hieringer, W.; Görling, A.; Autschbach, J. *J. Phys. Chem. A* **2005**, *109*, 4836.

(43) Fan, J.; Autschbach, J.; Ziegler, T. *Inorg. Chem.* **2010**, *49*, 1355.

(44) Mason, S. F. *Molecular Optical Activity & the Chiral Discriminations*; Cambridge University Press: Cambridge, U.K., 1982.

(45) Mason, S. F. *Inorg. Chim. Acta* **1968**, *2*, 89.

(46) Bosnich, B. *Acc. Chem. Res.* **1969**, *2*, 266.

(47) Daul, C.; Schlaepfer, C. W. *J. Chem. Soc., Dalton Trans.* **1988**, 393.

(48) Autschbach, J.; Nitsch-Velasquez, L.; Rudolph, M. *Top. Curr. Chem.* **2011**, *298*, 1.